Photothermal Single Particle Rutherford Scattering Microscopy

Markus Selmke and Frank Cichos*

Molecular Nanophotonics Group, Institute of Experimental Physics I, University of Leipzig, 04103 Leipzig, Germany

(Received 9 October 2012; revised manuscript received 7 December 2012; published 6 March 2013)

We demonstrate that the quantum-mechanical description of Rutherford scattering has a photonic counterpart in a new form of single particle photothermal microscopy. Using a split detector we provide experimental evidence that photons are deflected by a photothermal potential that is created by a local refractive index change around a heated nanoparticle. The deflection experienced is shown to be the analog to the deflection of a massive particle wave packet in unscreened spinless Coulomb scattering. The experimentally found focal detection geometry reveals a lateral split feature which will allow new correlation-based velocimetry experiments of absorbing particles with ultrahigh sensitivity.

DOI: 10.1103/PhysRevLett.110.103901 PACS numbers: 42.30.−d, 42.25.Bs, 42.25.Fx

Rutherford scattering, which is the scattering of α particles on atoms, has changed our picture of the structure of matter fundamentally. It has revealed that almost all of the mass of an atom is confined in a positively charged nucleus, which is 4 orders of magnitude smaller than the size of an atom. The physical problem that has been analyzed by Rutherford [1] is in a classical nonrelativistic picture the deflection of positively charged α particles by the positively charged nucleus of the scattering atom. His well-known description explained the experiments by Geiger and Mardsen [2] recording also backscattering events, meaning particles are even reflected by the scattering atom. This classical particle picture has been extended to a quantum-mechanical description since then [3], where the α particle is treated as a matter wave interacting with the nucleus of the scattering atom via Coulomb interactions. Here, we demonstrate that this quantum-mechanical Rutherford scattering owns an optical analog where photons are deflected by the interaction with a photothermal (PT) potential, which is the local dielectric function perturbation exploited in photothermal microscopy on single nano-objects, a vastly growing type of microscopy [4]. An experimental extension of PT detection using a quadrant photodiode detector directly reveals the deflection of light by the PT potential and creates a split focus geometry, which will find new application in the measurement of flows by (cross-)correlation spectroscopy [5–8].

The quantum-mechanical treatment of Rutherford scattering [3,9] is described by the stationary Schrödinger equation

$$\nabla^2\Psi_C^k(\mathbf{r}) + k^2\left[1 - \frac{2\nu}{kr}\right]\Psi_C^k(\mathbf{r}) = 0, \tag{1}$$

where the wave vector k of the incident particle wave is defined through the de Broglie relation $\hbar k = m v_0$ and $\nu = Ck/2E$ quantifies the interaction strength for a given positive total energy E and Coulomb force constant C. A positive value of $\nu > 0$ corresponds to a repulsive, and a negative $\nu < 0$ to an attractive potential. A solution of the wave equation is a plane wave that is distorted by the interaction with the scattering potential,

$$\Psi_C^{\mathbf{k}}(\mathbf{r}) = e^{-(\pi/2)\nu}e^{i\mathbf{k}\cdot\mathbf{r}}\Gamma(1 + i\nu)_1F_1(-i\nu; 1; i(kr - \mathbf{k}\cdot\mathbf{r})). \tag{2}$$

While Eq. (1) has been formulated to describe particle scattering with fixed mass, kinetic energy, and incidence direction along $\mathbf{k}$ [10], it is mathematically a scalar wave equation. Thus, it is in general valid for types of waves other than matter waves as well. Under specific circumstances, a correspondence to the propagation of light in an inhomogeneous medium may be found. A direct mapping can be formulated and applied to PT single particle microscopy [11–13]. This type of microscopy has recently been developed to image and characterize single absorbing nonfluorescent molecules and nanoparticles [4,14,15]. Using a heating laser to optically excite an almost pointlike absorber, the heat released generates a local temperature rise, which decays with the inverse distance r^{-1} from the particle. As a consequence of this local temperature rise, the refractive index n_0 of the surrounding material is changed as well according to $n(r) = n_0 + \Delta n R/r$ with the contrast $\Delta n = \Delta T dn/dT$ given by the thermorefractive coefficient dn/dT and the induced particle temperature rise ΔT. This delivers the photothermal potential, which is scattering a second focused probe laser beam that is not absorbed by the particle. To describe the interaction of this probe laser beam with the refractive index profile, one needs to solve the Helmholtz equation (HE) for weak perturbations [16]

$$\nabla^2 U(\mathbf{r}) + k^2[n(\mathbf{r})/n_0]^2 U(\mathbf{r}) = 0, \tag{3}$$

wherein U corresponds to the scalar electric field. As the thermorefractive coefficient dn/dT is typically on the order of $\mathcal{O}(-10^{-4}\ \mathrm{K}^{-1})$ and thus $|\Delta n/n_0| \ll 1$ we can approximate $[n(\mathbf{r})/n_0]^2$ by $1 + 2r^{-1}\Delta n R/n_0$ and obtain a

scalar HE [Eq. (4)], which is mathematically completely equivalent to the stationary Schrödinger equation (1)

$$\nabla^2 U_C^k(\mathbf{r}) + k^2\left[1 + \frac{2\Delta n R}{n_0 r}\right]U_C^k(\mathbf{r}) = 0. \tag{4}$$

This immediately implies that the distorted plane-wave solution in Eq. (2) is also the solution of the HE (4), substituting $\nu \rightarrow -k\Delta n R/n_0$. Thus, the overall light scattering problem employed in PT single particle microscopy is the optical analog of Rutherford scattering (attractive or repulsive).

Nevertheless, neither in PT detection nor in Rutherford scattering does the solution presented in Eq. (2) directly correspond to the actual signal measured. In both cases, the incident particles or photons do not occupy a plane-wave mode [10]. PT detection, for example, uses a focused Gaussian beam. To demonstrate the equivalence of both Rutherford and PT single particle detection, we model a focused beam at $\mathbf{r}_0$ as a wave packet, with similar properties as a TEM00-mode Gaussian beam, by a plane-wave superposition

$$U_0^{\mathrm{wp}}(\mathbf{r}) = \int d\mathbf{k} A(\mathbf{k}) e^{i\mathbf{k}\cdot(\mathbf{r}-\mathbf{r}_0)}, \tag{5}$$

with an azimuthally symmetric monochromatic wave-vector spectrum $A(\vartheta) = \delta(\bar{k}-k)\exp(-\vartheta^2/2\sigma_\vartheta^2)$ in spherical coordinates. Such a wave packet has a characteristic width scale given by $\omega_\vartheta = 2/[k\sigma_\vartheta]$ [17,18].

The deflected or diffracted probing beam is given by the superposition [10] of the plane-wave solutions Eq. (2):

$$U_C^{\mathrm{wp}}(\mathbf{r}) = \int d\mathbf{k} A(\mathbf{k}) e^{-i\mathbf{k}\cdot\mathbf{r}_0} U_C^{\mathbf{k}}(\mathbf{r}). \tag{6}$$

Using Eq. (6) one may reproduce the familiar classical limit of geometrical Rutherford scattering, which is obtained when considering the parametric ray solution to Fermat's least optical path principle $d^2\mathbf{r}/ds^2 = \nabla\frac{1}{2}n^2(\mathbf{r})$ with the stepping parameter s determined by $|d\mathbf{r}/ds| = n(\mathbf{r})$ [19]. This classical limit results in hyperbolic ray trajectories $r(\phi)$ [13] given by

$$1/r(\phi) \approx \left[\sqrt{b^2\xi^2+1}\cos(\phi-\phi_0) \pm 1\right]^{-1} \Big/ [|\xi| b^2] \tag{7}$$

in polar coordinates. Here, the appropriate sign $\pm 1 = -\xi/|\xi|$ is determined by sign of the interaction strength in $\xi = k/\nu$, which appears here in a wavelength independent combination. The ray trajectory has its closest approach to the scattering center at an angle $\phi_0 = \pi/2 + \arctan(1/b\xi)$ when the ray is incident with the impact parameter b. The familiar Rutherford trajectories for massive and charged particles, that is, the solution to Newton's equation of motion $md^2\mathbf{r}/dt^2 = -\nabla C r^{-1}$ for given total energy E, are entailed in Eq. (7) by the substitution $\xi \rightarrow 2E/C$. An interesting difference, however, is that in the optical case no backscattering will occur, because the ratio of the wavelength to the geometric closest approach distance, $\lambda/2\xi^{-1}$, is typically large, meaning that the wave will be diffracted by the central particle of radius R before backscattering by the PT potential can occur.

To obtain this classical limit equation (7) from Eqs. (6) and (5) one should choose a beam of a finite width ω_ϑ and small angular spread (i.e., paraxial) with a lateral offset $|\mathbf{r}_0|$ larger than its width scale. Such a stretched wave packet does not describe the wave packet's temporal trajectory as we consider a stationary solution only. However, an extension to pulses and matter wave packet dynamics is readily obtained by the inclusion of the factor $\exp(-i\omega_k t)$ in the integrand of Eq. (6) with $\omega_k = ck$ for light pulses [17] or $\omega_k = \hbar k^2/2m$ for matter wave packets [10] assuming some frequency dispersion. Without such a dispersion, Eq. (6) reflects the time averaged probability to find particles or photons at a spatial position. The beam will experience a deflection by the scattering angle $\theta = 2\phi_0 - \pi$, which fulfills the well-known relation $\cot(\theta/2) = b\xi$ [1]. Figure 1(a) displays such a narrow and small wavelength Gaussian wave packet, which is offset by $b \equiv |\mathbf{r}_0|$ from the optical axis. The shape of the wave packet clearly follows the classical limit indicated by the white line demonstrating the equivalence to the classical Rutherford

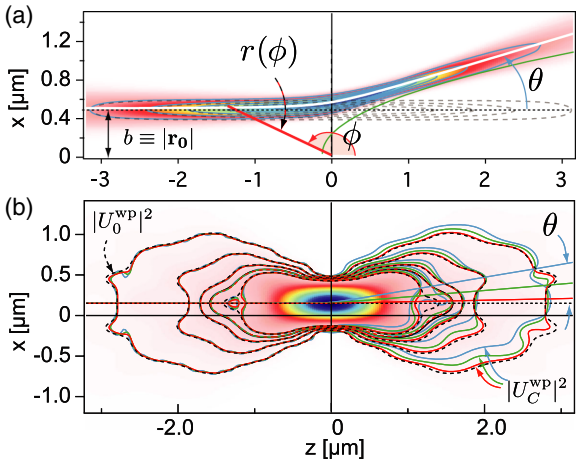

FIG. 1 (color online). (a) Deflection of a narrow Gaussian wave packet $|U_C^{\mathrm{wp}}|^2$, Eq. (6), on a PT potential. The following parameters have been used for the calculation: $\nu = 17.1$, $\bar{k} = 289\ \mu\mathrm{m}^{-1}$, $\mathbf{r_0} = 0.5\ \mu\mathrm{m}\hat{\mathbf{x}}$, $\sigma_\vartheta = 3°$, $\omega_\vartheta = 0.13\ \mu\mathrm{m}$. The white line corresponds to the classical Rutherford trajectory $r(\phi)$, Eq. (7). The dashed contour lines show the initial beam amplitude $|U_0^{\mathrm{wp}}|^2$, Eq. (5). (b) Off axis diffraction or deflection of a wide Gaussian wave packet $|U_0^{\mathrm{wp}}|^2$ (image, dashed contours) on a PT potential. The solid contour lines show the diffracted beams $|U_C^{\mathrm{wp}}|^2$ for varying interaction strengths $\nu = \{0.0214, 0.0855, 0.171\}$ (red, green, blue). Parameters: $n_0 = 1.46$, $dn/dT = -3.6\times10^{-4}\ \mathrm{K}^{-1}$, $\Delta T = \{200, 800, 1600\,\mathrm{K}\}$, $\lambda = 635$ nm, offset $\mathbf{r_0} = 0.150\ \mu\mathrm{m}\hat{\mathbf{x}}$, $\sigma_\vartheta = 27.7°$, $\omega_\vartheta = 0.286\ \mu\mathrm{m}$. The corresponding Rutherford trajectories are displayed in the appropriate color and have deflection angles $\theta \approx \{1.13°, 4.5°, 9.02°\}$.

scattering solution. This is the expected $\lambda \rightarrow 0$ classical limit of the wave-scattering description of light [20].

The experimental conditions in PT single particle microscopy, however, do not correspond to this limit. The beamwidth is in general larger than the characteristic lateral offset $|\mathbf{r}_0|$ of the probe beam. Therefore, without having a well-defined impact parameter, the Rutherford analogy becomes less apparent. Nevertheless, this situation is still covered by Eq. (6) inserting the appropriate wave packet and comprises the general features of a deflection of the incident wave packet. To demonstrate this we detect the deflection of the incident probe light on the PT potential by measuring the change (Δ) induced by the heating laser in the difference (δ) signals of a quadrant photodiode detecting transmitted powers P_d,

$$\Phi^i_{\mathrm{RF}} = \Delta(\delta_i P_d) = \delta_i P_d(\mathrm{hot}) - \delta_i P_d(\mathrm{cold}). \qquad (8)$$

The difference δ_i may be either between the left and right or top and bottom quadrants, $i = \{x, y\}$, respectively. This is in fact an extension of the thin sample slab transverse PT deflection spectroscopy [21] or mirage technique [22] in which a macroscopic layered refractive index field is probed. Here, however, the geometrical optics limits of Maxwell's equations cannot be used. The change Δ is most conveniently measured with the help of a lock-in amplifier that demodulates the respective probe-beam signals on the frequency of the heating beam intensity modulation. We demodulate either the sum signal of a quadrant photodiode to obtain the PT signal [11–13], $\Phi = \Delta P_d$, or the difference channels to get the the heat-induced Rutherford deflection signals, Φ^i_{RF}, corresponding to Eq. (8).

Accordingly, the experimentally found focal detection volumes of the PT signal Φ show an axially split detection volume [11–13], see Figs. 2(a) and 2(d), while the PT Rutherford scattering signals Φ^x_{RF} and Φ^y_{RF} have a lateral splitting, signifying the experienced deflection, see Figs. 2(b), 2(c), and 2(e). The xz and yz plane scans for the PT δ_y-channel signal are exemplarily shown in Fig. 2(e) for our diffraction limited focused probe and heating beams. Evidently, the spatial heating beam intensity distribution $I_h(\mathbf{r})$ also limits the spatial extent of the PT detection functions as it sets the interaction potential strength by $\nu \propto I_h$ [18]. The heating beam position relative to the probing beam determines which interaction is enhanced and thus determines the asymmetry of the spatial signal shape [11–13]. However, the type and working principle of interaction itself is only determined by the probe beam

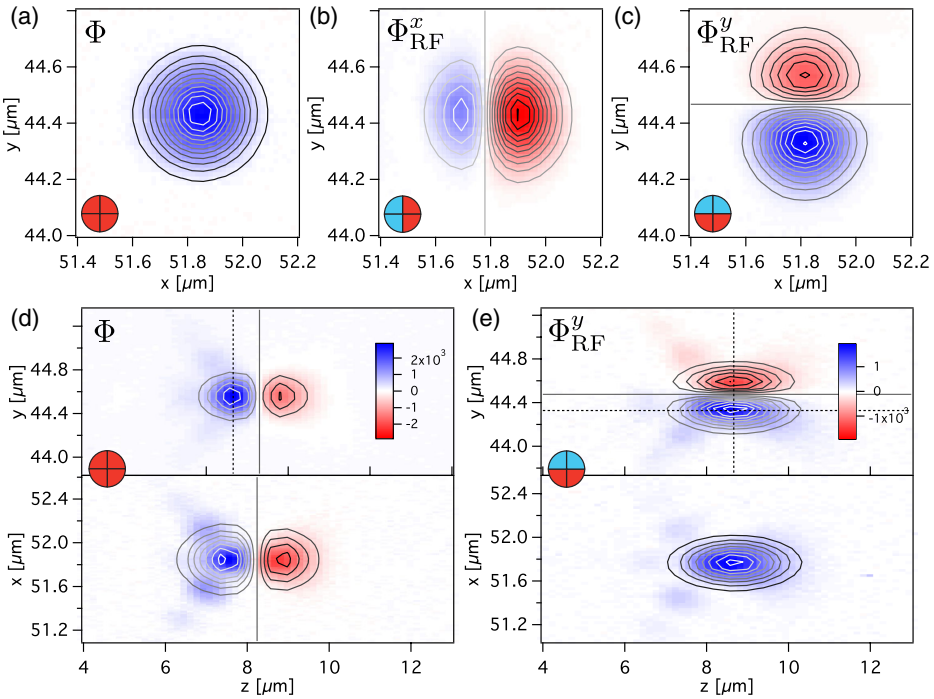

FIG. 2 (color online). PT images of a $R = 30$ nm AuNP in a scanning sample PT transmission microscope setup [18]. Heating ($\lambda = 532$ nm) and probe beam ($\lambda = 635$ nm) are focused with a $\mathrm{NA_{ill}} = 1.4$ oil immersion objective and collected with $\mathrm{NA}_d = 0.8$ dry objective. Embedding polymer was PDMS. (a), (b), (c) Experimental xy scans of the PT sum Φ and the PT Rutherford scattering microscopy detection volumes Φ^x_{RF} and Φ^y_{RF}. The fit parameters are $\omega_y = 207$ nm, $\Delta y = -40$ nm, $\omega_x = 225$ nm, $\Delta x = 28$ nm. (d, e) zx and zy scans of Φ and Φ^y_{RF}. The focus is only split in one lateral direction (here zy). In the perpendicular lateral direction (zx) it is the product of a lateral and axial Gaussian, see Eq. (9). Fit parameters as above and $\omega_z = 1.54$ μm, $\Delta z = 150$ nm.

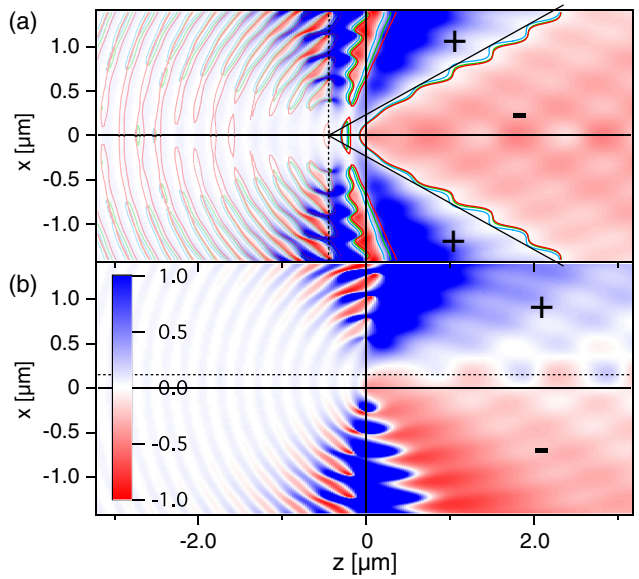

FIG. 3 (color online). Relative PT signal spatial distributions $[|U_0^{\mathrm{wp}}|^2 - |U_C^{\mathrm{wp}}|^2]/|U_0^{\mathrm{wp}}|^2$ for axially and laterally offset probe beams calculated for an incident Gaussian wave packet (see text). (a) negative axial offset $\mathbf{r_0} = -0.450\ \mu\mathrm{m}\hat{\mathbf{z}}$. A positive axial offset reverses the sign of the pattern [18]. (b) lateral offset probe beam as depicted in Fig. 1(b). Parameters and contour colors as in Fig. 1(b). Images and color scale correspond to $\nu = 0.171$.

interacting with the PT potential. The following empirical fit-functions describe this novel focal detection geometry:

$$\Phi_{(\mathrm{RF})}^{(i)} = \Phi_0^i[i - i_0 - \Delta i] \prod_{j=x,y,z} \exp\left(-\frac{2[j - j_0]^2}{\omega_j^2}\right), \quad (9)$$

with $i = x$ for the quadrant-diode x-difference signal Φ_{RF}^x, $i = y$ for the y-difference signal Φ_{RF}^y and $i = z$ for the sum signal Φ. The fit parameters $\{\Delta x, \Delta y, \Delta z\}$ take into account the actual heating to probe beam offset in the corresponding spatial directions. The fits according to Eq. (9) are shown as contours in Fig. 2.

Although a systematic quantification shall not be within the scope of this Letter, already the amplitude $\propto \nu$ of the normalized differences in these near-field diffraction calculations corresponds to the range of experimentally determined far-field relative PT signals [18]. The PT sum signal is best understood by looking at the diffraction pattern when the beam probes the refractive index profile on axis, see Fig. 3(a). An angular cone corresponding to the beam's spreading angle (lines) divides the spatial regions of positive and negative difference between the unperturbed $|U_0^{\mathrm{wp}}|$ and the diffracted beam $|U_C^{\mathrm{wp}}|$. The PT sum signal Φ corresponds to the interference zone that remains undetected in classical Rutherford scattering experiments where its angular extent, $\theta_i = \sqrt{\frac{\pi}{kr}}$, due to plane-wave—like incidence, vanishes at large distances [10]. Outside of this interference domain, the differential Rutherford cross-section $\frac{\mathrm{d}\sigma}{\mathrm{d}\Omega} = \frac{\nu^2}{4k^2}\sin^{-4}(\theta/2)$ is in contrast quadratic in the perturbation. For focused-wave diffraction, the angular spread of the plane-wave spectrum representing the probe beam broadens up the interference zone and describes the intensity (re)distribution detected in this scheme. The result is a focal volume split in an axial direction as seen in Fig. 2(d).

A probe beam with a finite displacement in a lateral direction will experience a deflection as seen in Fig. 1(b). The resulting relative PT deflection signal distribution, as shown in Fig. 3(b), is such that the difference between the initial probing beam and the diffracted beam shows positive and negative values on two sides of a dividing line approximately determined the symmetry axis of the initial beam. In an experiment, the use of a quadrant photodiode provides a PT signal that is only sensitive to exactly this deflection of the focused beam. While still present, the widening or collimation of the beam responsible for the ordinary PT signal will thereby not contribute. All PT signal recording schemes, whether the sum or difference signals are considered, are thereby special cases of the optical scalar wave counterpart to Rutherford scattering in its quantum-mechanical description. The wave-packet scattering hereby described is quantitatively fully consistent with the recent analytical on axis only analysis in terms of Fresnel-Kirchhoff diffraction [12,18].

We have experimentally demonstrated and theoretically explained a nanoscopic deflection-microscopy technique that provides a sharply split focus having two distinct lobes differing in sign of their respective PT signal. The signal generating mechanism in this novel detection scheme was shown to be the PT counterpart to quantum-mechanical Rutherford scattering of wave packets. The splitting may be achieved simultaneously in all three spatial directions by using and the difference channels $\delta_{x,y}P_d$ in x and y of a quadrant photodiode in a PT transmission microscopy setup and allows the distinction of particle positions occupying any of the eight octants relative to the focus of the probe beam. The possible applications range from 3D velocimetry in microstructured flow channels (via cross-correlation functions akin to Ref. [8]) to feedback controlled PT particle tracking. The achieved reframing of a generalized PT signal further opens the path to future inquiries on the nanoscopic temperature distribution around heated nanoparticles through the powerful toolbox of potential scattering in quantum mechanics.

Financial support by the DFG research unit 877 "From local Constraints to Macroscopic Transport" is acknowledged.

*cichos@physik.uni-leipzig.de
http://www.uni-leipzig.de/~physik/mona.html

[1] E. Rutherford, Philos. Mag. **21**, 669 (1911).
[2] H. Geiger and E. Marsden, Proc. R. Soc. A **82**, 495 (1909).

[3] W. Gordon, Z. Phys. **48**, 180 (1928).
[4] A. Gaiduk, M. Yorulmaz, P. V. Ruijgrok, and M. Orrit, Science **330**, 353 (2010).
[5] V. Octeau, L. Cognet, L. Duchesne, D. Lasne, N. Schaeffer, D. G. Fernig, and B. Lounis, ACS Nano **3**, 345 (2009).
[6] P. M. R. Paulo, A. Gaiduk, F. Kulzer, S. F. G. Krens, H. P. Spaink, T. Schmidt, and M. Orrit, J. Phys. Chem. C **113**, 11 451 (2009).
[7] R. Radünz, D. Rings, K. Kroy, and F. Cichos, J. Phys. Chem. A **113**, 1674 (2009).
[8] M. Selmke, R. Schachoff, M. Braun, and F. Cichos, RSC Adv. **3**, 394 (2013).
[9] L. D. Landau and E. M. Lifschitz, *Quantenmechanik*, Lehrbuch der Theoretischen Physik Vol. III (Akademie-Verlag, Berlin, 1988), 8th ed.
[10] V. G. Baryshevskii, I. D. Feranchuk, and P. B. Kats, Phys. Rev. A **70**, 052701 (2004).
[11] M. Selmke, M. Braun, and F. Cichos, ACS Nano **6**, 2741 (2012).
[12] M. Selmke, M. Braun, and F. Cichos, Opt. Express **20**, 8055 (2012).
[13] M. Selmke, M. Braun, and F. Cichos, J. Opt. Soc. Am. A **29**, 2237 (2012).
[14] S. Berciaud, L. Cognet, G. A. Blab, and B. Lounis, Phys. Rev. Lett. **93**, 257402 (2004).
[15] D. Rings, R. Schachoff, M. Selmke, F. Cichos, and K. Kroy, Phys. Rev. Lett. **105**, 090604 (2010).
[16] B. E. A. Saleh and M. C. Teich, *Fundamentals of Photonics*, Wiley Series in Pure And Applied Optics (John Wiley and Sons, Inc., New York, 1991).
[17] W. Zakowicz, Europhys. Lett. **85**, 40001 (2009).
[18] See Supplemental Material at http://link.aps.org/supplemental/10.1103/PhysRevLett.110.103901 for experimental setup and theory details and perspectives on the signal quantification.
[19] J. Evans and M. Rosenquist, Am. J. Phys. **54**, 876 (1986).
[20] W. Zakowicz, J. Phys. A Math. Gen. **36**, 4445 (2003).
[21] W. B. Jackson, N. M. Amer, A. C. Boccara, and D. Fournier, Appl. Opt. **20**, 1333 (1981).
[22] J. C. Murphy and L. C. Aamodt, J. Appl. Phys. **51**, 4580 (1980).